

1 **PFOA and PFOS removal by ion exchange for water reuse and drinking applications: Role**
2 **of organic matter characteristics**

3 Fuhar Dixit^a, Benoit Barbeau^b, Shadan Ghavam Mostafavi^c, Madjid Mohseni^{a*}

4 ^{a,c} Department of Chemical and Biological Engineering, University of British Columbia,
5 Vancouver, Canada

6 ^b Department of Civil, Geological and Mining Engineering, Polytechnique Montreal, Montreal,
7 Quebec, Canada

8

9 **Supplementary Information**

10

11 **S.1 Trace Minerals for Synthetic Effluent**

12 Details on the addition of trace minerals for the preparation of synthetic effluents is presented
13 below.

14

15 Table S.1 Details on trace minerals utilized for preparing the synthetic effluents

Chemical	Stock Volume	Added mass (g)	Volume Added to 1 L final solution
Trace Minerals			
FeSO ₄ ·7H ₂ O	2L	6.06	2 mL
ZnSO ₄ ·7H ₂ O		0.63	
CuSO ₄ ·5H ₂ O		0.11	
CoCl ₂ ·6H ₂ O		0.11	
H ₃ BO ₃		0.10	
KI		0.10	
NiCl ₂ ·6H ₂ O		0.04	
Al ₂ (SO ₄) ₃ ·18H ₂ O		0.27	
MnCl ₄ ·4H ₂ O		0.56	
Na ₂ EDTA		13.73	
Na ₂ EDTA		13.73	

16

17

18

19 Table S.2. Details on other chemical species used for the preparation of synthetic effluents

20

Chemical	Stock Volume	Added mass (g)	Volume Added to 1 L final solution
Phosphorous			
Na ₂ HO ₄ ·7H ₂ O	2L	307.66	2 mL
KH ₂ PO ₄		100.00	
Alkalinity			
NaHCO ₃	1.5 L		8 mL
Ammonia			
NH ₄ Cl	2L		2 mL

21

22

23

24

25

26

27

28

29

30

31

32

33

34

35

36

37

38

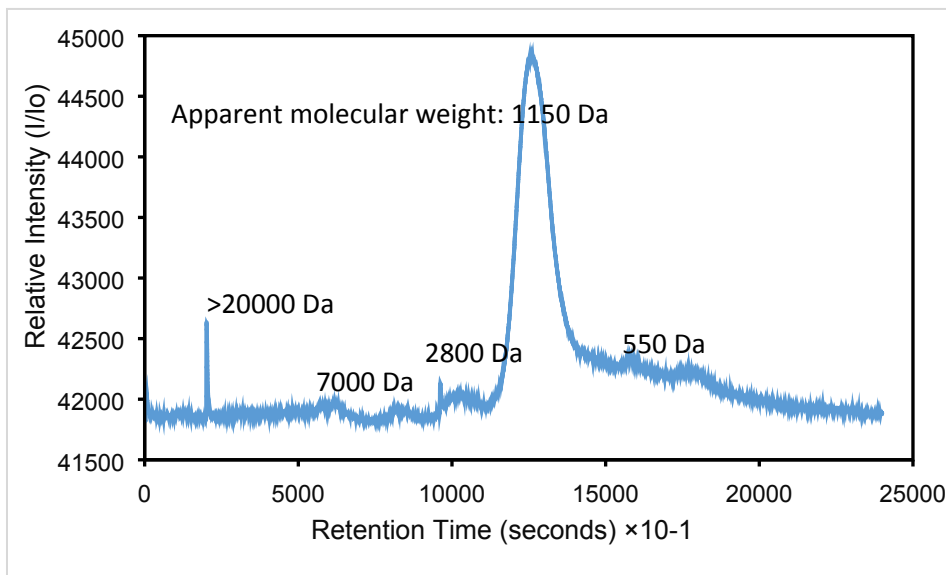
39

40

41

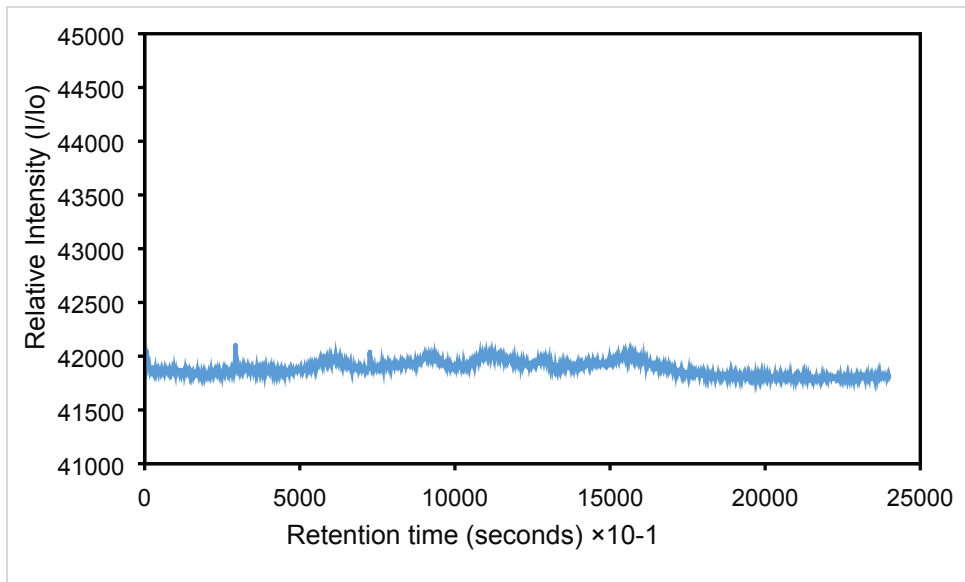
42 **S.2 LCOCD data for natural waters**

43 LCOCD was performed using HPLC (Perkin Elmer, Canada) with 900 Turbo Potable OC
44 Analyzer (detection range: 0.2-10 mg C/L, GE Sievers, Canada) for analysis of the source water
45 NOM using the previously described method ¹⁻³. Note, the LCOCD graphs for wastewaters were
46 obtained using a Waters C-8 column while the LCOCD graphs for NOM isolates and surface
47 waters were obtained on a Waters C-18 column resulting in different elution times for
48 corresponding molecular weights.



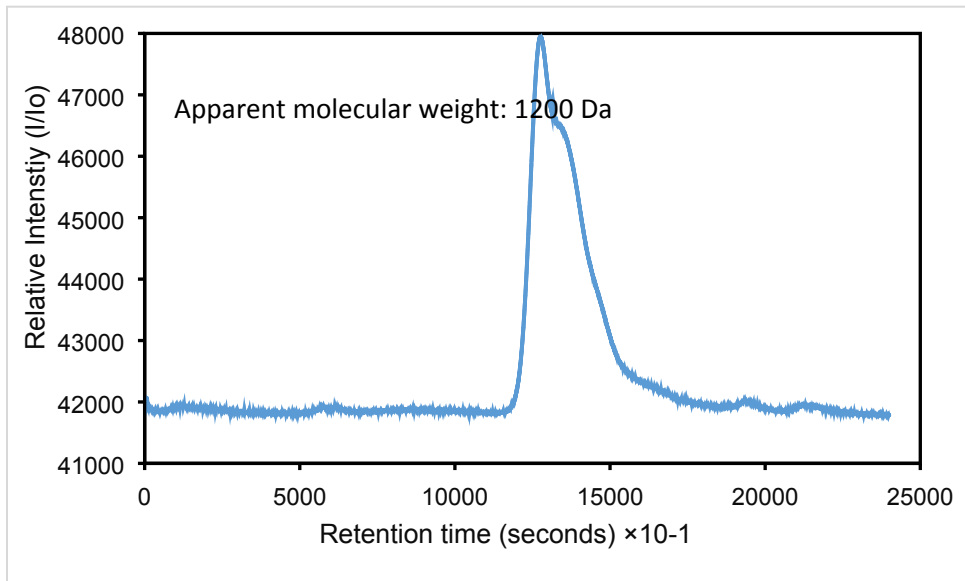
49

50 Figure S.1 LCOCD data for Vancouver Convention Centre Water before IX treatment.



51

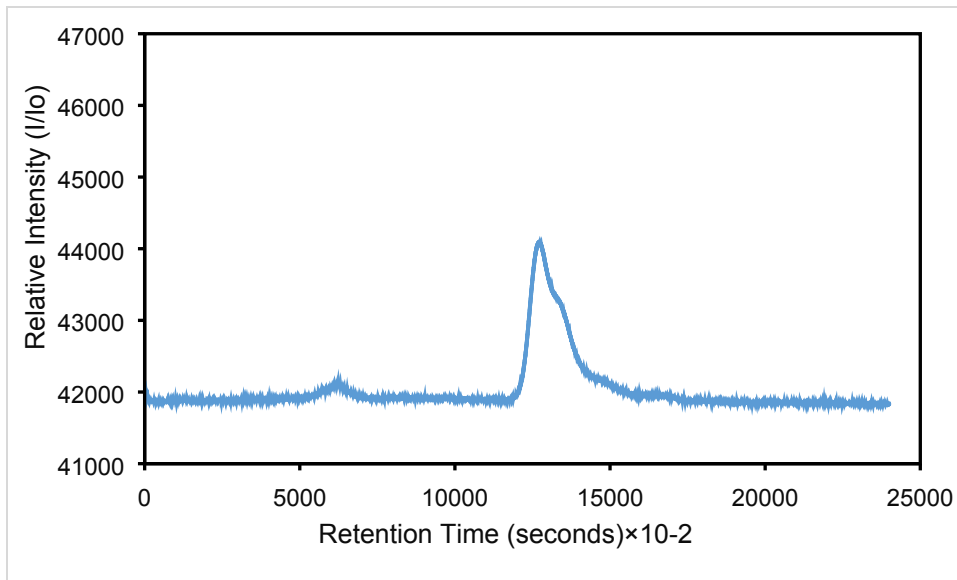
52 Figure S.2 LCOCD data for Vancouver Convention Centre Water after IX treatment (IX: 500
 53 mg/L, 24 hours).



54

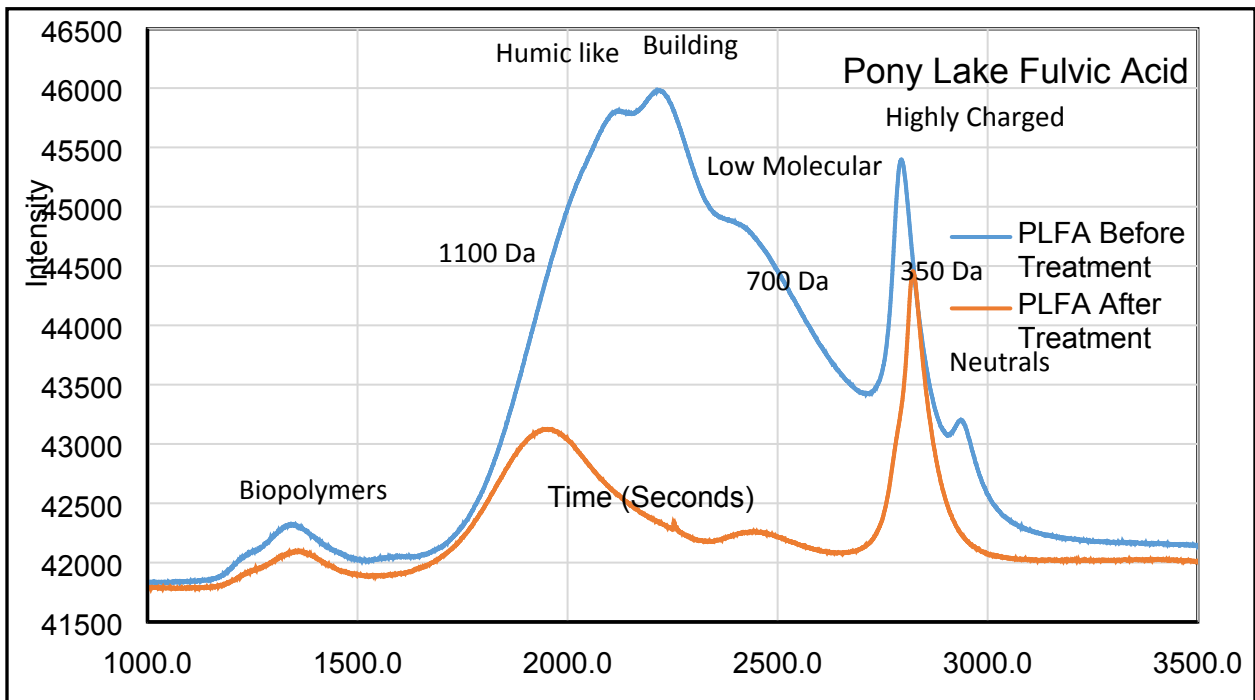
55 Figure S.3 LCOCD data for Synthetic effluent prepared at the UBC environmental laboratory
 56 before IX treatment.

57



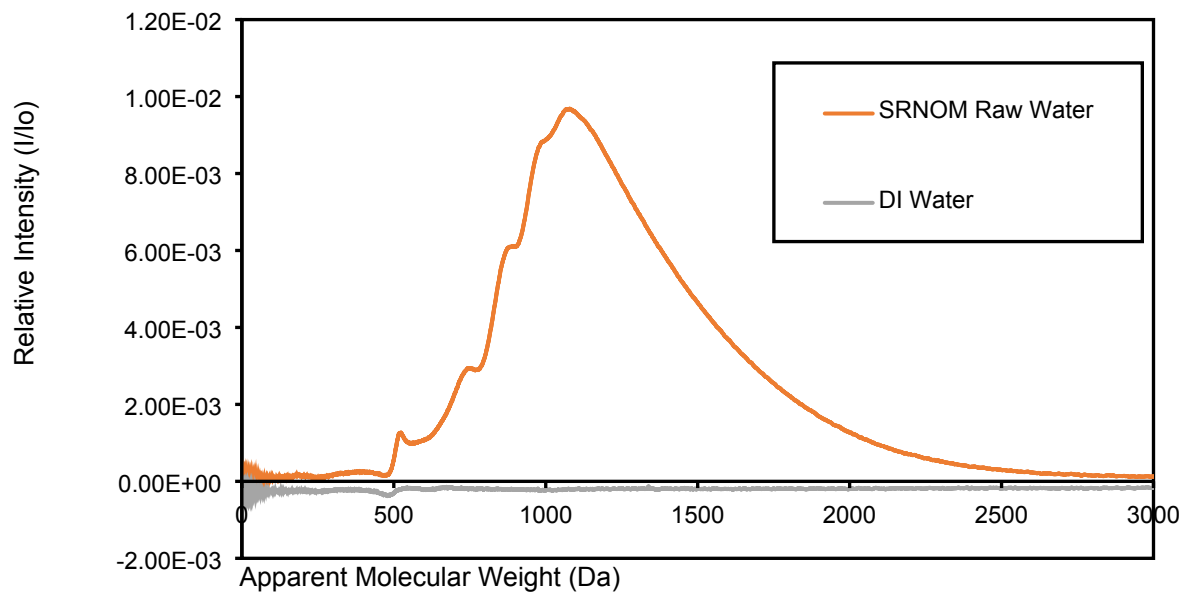
58

59 Figure S.4 LCOCD data for Synthetic effluent prepared at the UBC environmental laboratory
 60 after IX treatment (500 mg/L IX, 24 hours).



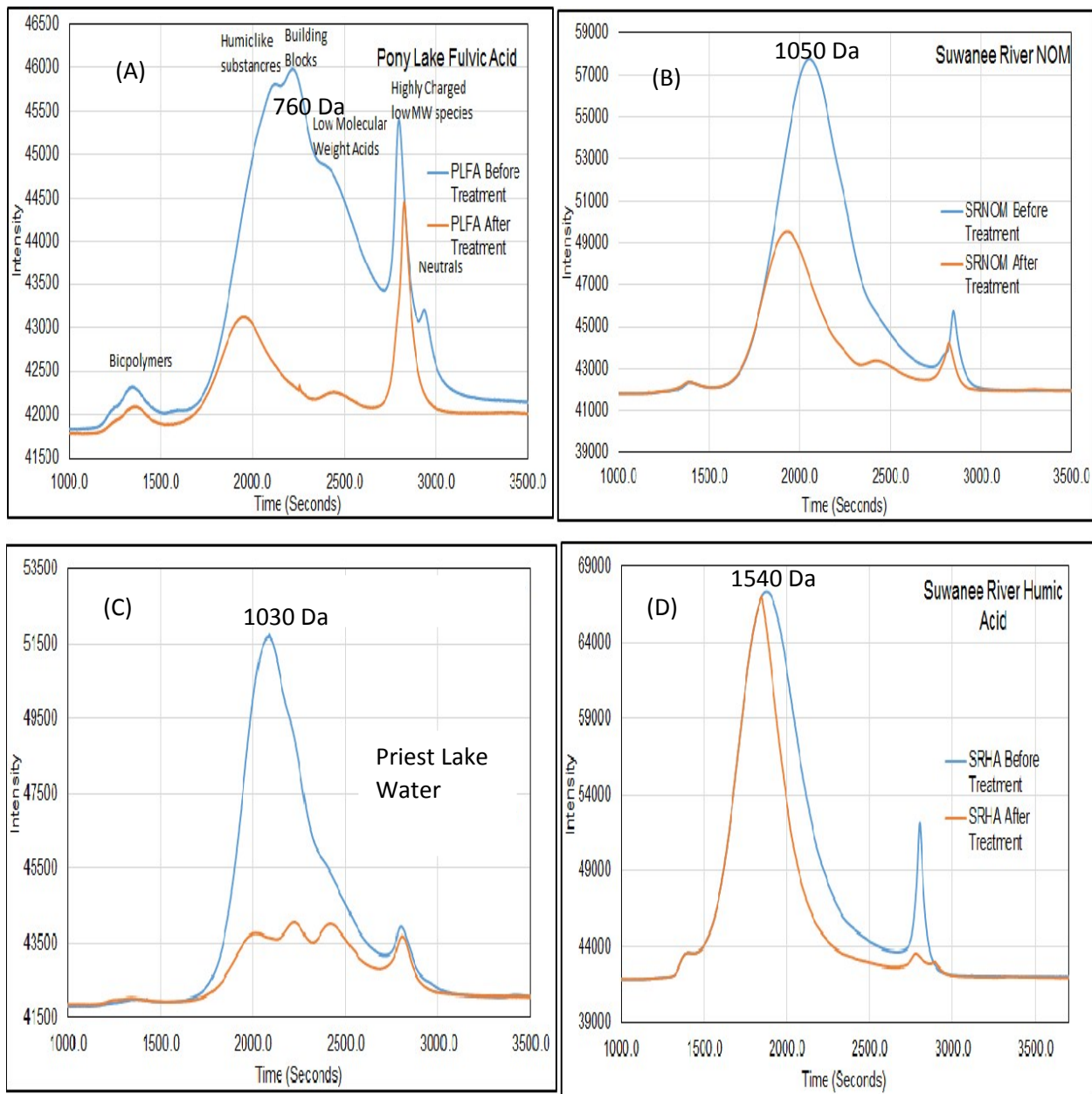
61

62 Figure S.5 LC-OCD graph for Pony Lake Fulvic Acid before and after IX treatment. (X axis
 63 represents elution time). IX dosage of 100 mg/L (or 0.45 mL/L).



64

65 Figure S.6 LC-OCD graph for Suwanee River NOM plotted as a function of apparent molecular
66 weight.



67

68 Figure S.7 Comparative LCOCD graphs for (A) PLFA, (B) SRNOM, (C) Priest Lake (Natural
 69 Surface Water, Vancouver Island, BC, Canada), (D) SRHA.

70 *Treated with IX dosage of 100 mg/L (or 0.45 mL/L)

71

72

73 S.3 Vancouver Convention Centre (VCC) Plant

74

75 The VCC treatment process comprises of a conventional activated sludge process followed by a
76 treatment with membrane bioreactor. The plant treats grey and black water from the building.
77 The treated water is used back in the washrooms for toilet flushing and rooftop irrigation during
78 summer and warmer months.

79

80

81 S.4 Equivalent Background Concentration Model

82

83 The EBC parameters (K_{EBC} , $1/n_{EBC}$ and C_{oEBC}) were determined according to the procedure
84 described elsewhere^{2,4}. The multicomponent interactions are predicted using the ideal adsorbed
85 solution theory (IAST) which results in Eqs. 3.3 and 3.4, where K_{EBC} and $1/n_{EBC}$ are the Freundlich
86 single solute isotherm parameters for EBC and K_m and $1/n_m$ are single solute isotherm parameters
87 for the micropollutants. Measured concentrations were fitted to Eqs. 3.3 and 3.4 by using non-
88 linear optimization schemes^{5,6}.

$$89 \quad C_{me} = \frac{q_{me}}{q_{me} + q_{EBCe}} \left(\frac{n_m \times q_{me} + n_{EBC} \times q_{EBCe}}{n_m \times K_m} \right)^{\times n_m}$$

90 (3.3)

$$91 \quad C_{EBCe} = \frac{q_{EBCe}}{q_{me} + q_{EBCe}} \left(\frac{n_m \times q_{me} + n_{EBC} \times q_{EBCe}}{n_{EBC} \times K_{EBCe}} \right)^{\times n_{EBC}}$$

92 (3.4)

93 The obtained EBC concentrations of respective compounds C_{EBC} in $\mu\text{eq/L}$, are summarized in
 94 Table 1.

95 The multicomponent interactions were further investigated as ⁷:

$$(C_{i,0} - q_i C_{IX}) - \frac{q_i}{\sum_{j=1}^N q_j} \left(\frac{\sum_{j=1}^N n_j q_j}{n_i K_i} \right)^{n_i} = 0, \quad i = 1 \dots N$$

96 (3.5)

97 where subscript i represents the target component, N is the number of components (e.g., in a binary
 98 system, $N=2$, $i = 1$ for MCLR, and $i = 2$ for EBC), K_i and n_i represent the single-solute Freundlich
 99 constants, $C_{i,0}$ is the initial concentration of component i ($\mu\text{eq/L}$), C_{IX} is the IX dosage (meq/L) and
 100 q_i is the solid phase concentration ($\mu\text{mol/meq}$). The model predictions were made by performing
 101 a non-linear optimization scheme as described elsewhere ⁸.

102 The multicomponent interactions were further investigated as ^{7,9}:

$$(C_{i,0} - q_i C_{IX}) - \frac{q_i}{\sum_{j=1}^N q_j} \left(\frac{\sum_{j=1}^N n_j q_j}{n_i K_i} \right)^{n_i} = 0, \quad i = 1 \dots N$$

103 11

104 where subscript i represents the target component, N is the number of components (e.g., in a binary
 105 system, $N=2$, $i = 1$ for GenX, and $i = 2$ for EBC), K_i and n_i represent the single-solute Freundlich
 106 constants, $C_{i,0}$ is the initial concentration of component i ($\mu\text{eq/L}$), C_{IX} is the IX dosage (meq/L) and
 107 q_i is the solid phase concentration ($\mu\text{mol/meq}$).

108 For instance in a binary system, with say GenX in presence of Suwannee River NOM only, we get
 109 the following

$$110 \quad C_{1,0} - q_1 C_{IX} - \frac{q_1}{q_1 + q_2} \left(\frac{n_1 q_1 + n_2 q_2}{n_1 K_1} \right)^{n_1} = 0,$$

111 12

$$112 \quad C_{2,0} - q_2 C_{IX} - \frac{q_2}{q_1 + q_2} \left(\frac{n_1 q_1 + n_2 q_2}{n_1 K_2} \right)^{n_2} = 0,$$

113 13

114 Where, subscript (i=1 or 2) represents GenX and the EBC, K_i and n_i represent the single-solute
 115 Freundlich constants, $C_{i,0}$ is the initial concentration of the component i ($\mu\text{g/L}$), C_{IX} is the IX
 116 dosage (g/L) and q_i is the solid phase concentration ($\mu\text{mol/L}$). As shown in equations 11 and 12,
 117 besides the adsorption parameters for the target compound ($C_{1,0}$, K_1 and n_1), three more EBC
 118 parameters ($C_{2,0}$, K_2 and n_2) are needed for the model prediction. These EBC parameters can be
 119 acquired using a non-linear optimization algorithm that could simultaneously solve the IAST
 120 equations as previously described^{8,10}. In sum, it can be started with assumption of initial values
 121 and assigning a small step change that can be added in recurring loops until the desired set of
 122 values fit the model within a range of permissible error (predefined value of say 0.01% error).

123 To evaluate the difference between model predictions and experimental data Marquardt's percent
 124 standard deviation (MPSD)¹¹ was used to predict the equilibrium adsorption data:

$$125 \quad \left(MPSD = 100 \sqrt{\frac{1}{m-p} \sum_{i=1}^p \left(\frac{q_e^{exp} - q_e^{cal}}{q_e^{exp}} \right)^2} \right)$$

126 where m is the number of experimental measurements and p is the number of parameters in the
 127 competitive isotherm. A smaller MPSD value (generally <10) corresponds to a better fit and lower
 128 error for the respective isotherm.

129 *Note, do not get confused with the MPSD error which relates to the error of experimental data
 130 and model predictions with the error value (say the 0.01%) previously defined to obtain EBC
 131 values during non-linear programming. The error value (of say 0.01%) is utilized only to get the
 132 best possible values for the three EBC parameters that can fit the model with least error (here
 133 0.01%). You may assign 0.001 % over 0.01% to get even better fits, it would just incur longer
 134 program runs to get the specified values.

135

136

137

138 **S.5 Resin micro porosity data**

139

140 Table S.3. Resin porosimetry results for IX resin (Purolite A860) and dimensions of SRFA and
 141 PFOA ²

Pore Size	Cumulative Pore Area (m^2/g) $\times 10^{-3}$	Pore Volume (mL/g) $\times 10^{-2}$	Pore Area (%)	Pore Volume (%)
Macropores (>50 nm)	1.0	3.1	< 0.1	18
Mesopores (2-50 nm)	5.3	4.3	25.3	26
Micropores (<2nm)	15.6	9.0	74.6	56
Dimensions of MCLR and SRFA				
Molecule	Size Range (nm)		Median (nm)	
SRFA ¹²	0.8-5		2 nm	

142

143

144 S.6 Inorganic Ion Removal

145 Table S.4. Initial and final concentrations of inorganic ions from VCC water vbefore and ater IX
146 treatment.

Inorganic ion	Nitrate	Sulphate	Phosphate
Initial Concentration (mg/L)	26.1 ± 0.2	32.3 ± 0.5	10.4 ± 0.3
Concentration after IX treatment (mg/L)	7.2 ± 0.5	2.6 ± 0.6	1.8 ± 0.2
Percentage Removal (%)	72 ± 2	92 ± 2	84 ± 2

147

148

149

150 S.7 Estimation of diffusion coefficients and Biot number

151 The analytical solution for intraparticle diffusion model (IDM) for single sized resin beads in a
152 completely stirred tank reactor are described by the following equations:

$$153 \quad Ut = \frac{C_o - C_t}{C_o - C_e} = \frac{q_t}{q_e} = 1 - \sum_{n=1}^{\infty} \omega \frac{6(\omega + 1)}{9 + 9\omega + \beta_n^2 \omega^2} \times \exp\left(-\frac{D_{a,1} \beta_n^2 t}{R_p^2}\right)$$

154 1

155 ω is calculated from:

$$156 \quad \frac{q_e}{VC_o} = \frac{1}{1 + \omega}$$

2

157 β_n are non – zero roots of the equation:

158
$$\tan \beta_n = \frac{3\beta_n}{1 + \omega\beta_n^2}$$

3

159

160 Where $U(t)$, is the fractional attainment of equilibrium and C_o , C_t and C_e are concentrations of
 161 solute (mg/L) at time $t=0$, at time t , and at equilibrium, respectively. R_p is the radius of the resin
 162 (assumed spherical, 0.375 cm) and $D_{a,l}$ is the apparent diffusivity ((cm²/s).

163 As opposed to intraparticle diffusion, the following equation represents the changes in the MCLR
 164 concentration for the case of film diffusion controlled removal:

165
$$U(t) = 1 - \exp\left(-\frac{3 \cdot D_f \cdot (V' C' + V C_o)}{R_p \cdot \delta \cdot C' V}\right)$$

166 4

167 Where C' is the resin exchange capacity (meq/L), δ is the film thickness (10⁻³ cm¹³), C_o is the
 168 initial solute concentration (meq/L), V is the solution volume (L), V' is the resin volume (L), D_f is
 169 the film diffusion coefficient (cm²/s).

170 For both IPD and film diffusion models, D_f or $D_{a,l}$ are assumed to be constant and are estimated
 171 based on nonlinear optimization schemes.

172 The curve fitted for D_f agreed well with the experimental data ($0.95 < R^2 < 0.98$), while the quality
 173 of fit for the pore diffusion model ($0.96 < R^2 < 0.99$), was well fitted under the dilute condition
 174 assumption, as described elsewhere¹³.

175 The rate-controlling step was further investigated using the dimensionless Biot number (Bi) which
176 is the ratio of internal mass transfer (i.e., pore diffusion) to external mass transfer (i.e. film
177 diffusion) resistances ¹⁴

$$178 \quad Bi = \frac{k_f \cdot R_p}{D_{pe}} \quad 5$$

179 where k_f (cm/s) is the external mass transfer coefficient ($k_f = D_f/\delta$) and D_f (cm²/s), is the film
180 diffusion coefficient and D_{pe} (cm²/s) is the effective pore diffusion coefficient (δ is film thickness
181 $\approx 10^{-3}$ cm according to ¹⁵. The $Bi \ll 1$ indicates film diffusion as the rate-limiting step where Bi
182 $\gg 1$ shows pore diffusion to be the rate limiting step.

183

184 D_a accounts for free liquid diffusion (D_l) and sorption to resins resistances, and tortuous
185 diffusion pathway through inside the resins and is correlated to effective pore diffusivity ($D_{p,e}$) as
186 follows (Weber Jr and DiGiano, 1996):

187

$$188 \quad D_a = \frac{D_l \cdot \varepsilon / \tau}{[(1 - \varepsilon)\rho_s K_D + \varepsilon]} = \frac{D_{pe} \cdot \varepsilon}{[(1 - \varepsilon)\rho_s K_D + \varepsilon]} \quad 6$$

189

190 Where K_D is the linear equilibrium partition coefficient, ε is the resin porosity ~ 0.46 ¹³, τ is the
191 tortuosity of the resin and is estimated to be ~ 3 ^{13,16,17}. ρ_s is solid phase density of 1.08 g/cm³
192 (manufacturer), and $D_{p,e}$ is effective pore diffusion coefficient (cm²/s).

193 ε/τ accounts for reduction in D_l because of the tortuosity of the diffusion path and the term $[(1-\varepsilon)$
194 $\rho_s K_D + \varepsilon]$ is referred to as retardation factor, by which the liquid diffusivity is reduced due to
195 local microscale partitioning. Assuming a linear distribution of toxin between the solid and liquid
196 phases was plausible because of the low concentrations of the solute (i.e, $\sim 1-100 \mu\text{g MCLR/L}$).
197 The R^2 values obtained for the linear correlation were between 0.92-0.98^{2,13}.

198

199

200 **References**

- 201 (1) Huber, S. A.; Balz, A.; Abert, M.; Pronk, W. Characterisation of Aquatic Humic and Non-
202 Humic Matter with Size-Exclusion Chromatography – Organic Carbon Detection –
203 Organic Nitrogen Detection (LC-OCD-OND). *Water Res.* **2011**, *45* (2), 879–885.
- 204 (2) Dixit, F.; Barbeau, B.; Mohseni, M. Characteristics of Competitive Uptake between
205 Microcystin-LR and Natural Organic Matter (NOM) Fractions Using Strongly Basic
206 Anion Exchange Resins. *Water Res.* **2018**, *139*, 74–82.
- 207 (3) Winter, J.; Wray, H. E.; Schulz, M.; Vortisch, R.; Barbeau, B.; Bérubé, P. R. The Impact
208 of Loading Approach and Biological Activity on NOM Removal by Ion Exchange Resins.
209 *Water Res.* **2018**, *134*, 301–310.
- 210 (4) Newcombe, G.; Morrison, J.; Hepplewhite, C. Simultaneous Adsorption of MIB and
211 NOM onto Activated Carbon. I. Characterisation of the System and NOM Adsorption.
212 *Carbon N. Y.* **2002**, *40* (12), 2135–2146.
- 213 (5) Ebie, K.; Li, F.; Azuma, Y.; Yuasa, A.; Hagishita, T. Pore Distribution Effect of Activated
214 Carbon in Adsorbing Organic Micropollutants from Natural Water. *Water Res.* **2001**, *35*

- 215 (1), 167–179.
- 216 (6) Matsui, Y.; Yoshida, T.; Nakao, S.; Knappe, D. R. U.; Matsushita, T. Characteristics of
217 Competitive Adsorption between 2-Methylisoborneol and Natural Organic Matter on
218 Superfine and Conventionally Sized Powdered Activated Carbons. *Water Res.* **2012**, *46*
219 (15), 4741–4749.
- 220 (7) Bunmahotama, W.; Hung, W. N.; Lin, T. F. Prediction of the Adsorption Capacities for
221 Four Typical Organic Pollutants on Activated Carbons in Natural Waters. *Water Res.*
222 **2017**, *111*, 28–40.
- 223 (8) Crittenden, J. C.; Sanongraj, S.; Bulloch, J. L.; Hand, D. W.; Rogers, T. N.; Speth, T. F.;
224 Ulmer, M. Correlation of Aqueous-Phase Adsorption Isotherms. *Environ. Sci. Technol.*
225 **1999**, *33* (17), 2926–2933.
- 226 (9) Dixit, F.; Barbeau, B.; Mohseni, M. Microcystin-LR Removal by Ion Exchange:
227 Investigating Multicomponent Interactions in Natural Waters. *Environ. Pollut.* **2019**, *253*,
228 790–799.
- 229 (10) Najm, I. N.; Snoeyink, V. L.; Richard, Y. Effect of Initial Concentration of a SOC in
230 Natural Water on Its Adsorption by Activated Carbon. *J. Am. Water Works Assoc.* **1991**,
231 *83* (8), 57–63.
- 232 (11) Kumar, K. V.; Porkodi, K.; Rocha, F. Comparison of Various Error Functions in
233 Predicting the Optimum Isotherm by Linear and Non-Linear Regression Analysis for the
234 Sorption of Basic Red 9 by Activated Carbon. *J. Hazard. Mater.* **2008**, *150* (1), 158–165.
- 235 (12) Wells, M. Conductivity-Dependent Flow Field-Flow Fractionation of Fulvic and Humic

- 236 Acid Aggregates. *Chromatography* **2015**, 2 (3), 580–593.
- 237 (13) Bazri, M. M.; Mohseni, M. Impact of Natural Organic Matter Properties on the Kinetics of
238 Suspended Ion Exchange Process. *Water Res.* **2016**, 91, 147–155.
- 239 (14) Ko, D. C. K.; Porter, J. F.; McKay, G. Film-Pore Diffusion Model for the Fixed-Bed
240 Sorption of Copper and Cadmium Ions onto Bone Char. *Water Res.* **2001**, 35 (16), 3876–
241 3886.
- 242 (15) Helfferich, F. Ion-Exchange Kinetics. V. Ion Exchange Accompanied by Reactions. *J.*
243 *Phys. Chem.* **1965**, 69 (4), 1178–1187.
- 244 (16) Li, P.; Sengupta, A. K. Intraparticle Diffusion during Selective Ion Exchange with a
245 Macroporous Exchanger. *React. Funct. Polym.* **2000**, 44, 273–287.
- 246 (17) Li, P.; SenGupta, A. K. Intraparticle Diffusion during Selective Sorption of Trace
247 Contaminants: The Effect of Gel versus Macroporous Morphology. *Environ. Sci. Technol.*
248 **2000**, 34 (24), 5193–5200.
- 249
- 250